Bull. Chem. Soc. Ethiop. **2025**, 39(6), 1057-1070.
DOI: https://dx.doi.org/10.4314/bcse.v39i6.3

ISSN 1011-3924
Printed in Ethiopia
Online ISSN 1726-801X

ENHANCING EFFICIENCY AND THERMAL STABILITY OF AMINO BENZOTRIAZOLE FLUORESCENT DYE VIA LIGAND-TO-METAL CHARGE TRANSFER REACTIONS FOR SOLAR CELL APPLICATIONS: A COMPREHENSIVE COMPOSITIONAL AND SPECTROSCOPIC STUDY

Mohamed Y. El-Sayed[1*], I.M. Ahmed[1], Tamer H.A. Hasanin[1], Moamen S. Refat[2], Y.F. El-Aryan[3] and Ivo Grabchev[4]

[1]Department of Chemistry, College of Science, Jouf University, Sakaka 2014, Saudi Arabia
[2]Department of Chemistry, College of Science, Taif University, P.O. Box 11099, Taif 21944, Saudi Arabia
[3]Department of Chemistry, College of Science, University of Bisha, P.O. Box 511, Bisha 61922, Saudi Arabia
[4]Chemistry and Biochemistry, Physiology and Pathophysiology, Faculty of Medicine, University of Sofia, 1407 Sofia, Bulgaria

(Received February 3, 2025; Revised February 27, 2025; Accepted March 3, 2025)

ABSTRACT. Herein in this study, we have synthesized three new iron(III), chromium(III), and vanadium(III) transition metal complexes of the 2-(2'-hydroxy-5'-phenyl)-5-aminobenzotriazole (hpabt) fluorescent dye. Infrared, and ultraviolet-visible spectral examinations, as well as elemental analysis, magnetic susceptibility, and molar conductivity analyses, all supported the structural interpretations. The complexes have a stoichiometry of 1:1 (M^{3+}: hpabt) based on the analytical, spectroscopic, and thermal data. The molar conductance measurements showed that the chloride ions inside the coordination sphere and all the metal chelates are non-electrolytes. These three complexes decomposition processes are examined and their thermal stabilities were examined using thermogravimetric (TGA) analysis. Activation entropy (ΔS*), activation enthalpy (ΔH*), free energy of activation (ΔG*), pre-exponential factor (A), and energy of activation (E*) are examples of kinetic parameters that have been recorded. The surface morphology of iron(III), chromium(III), and vanadium(III) complexes were studied by scanning electron microscopy (SEM). The 2-(2'-hydroxy-5'-phenyl)-5-aminobenzotriazole photostability as a fluorescent dye and its synthesized metal complexes doped in polymethyl methacrylate (PMMA) were subjected to UV-Vis. light, and the absorption spectra changed at various points during the exposure period.

KEY WORDS: Benzotriazole, Fluorescent dye, Transition metals, Thermal stabilities, Spectroscopic analyses

INTRODUCTION

Even though organic photochemistry has a long history [1], the development of photo-redox catalysis in the past ten years has altered synthetic chemists' perspectives on photochemistry [2, 3]. Today, the community has accepted the remarkable ability of light as a clean, selective, and potent source of energy to perform chemical reactions, and it is widely acknowledged in the field of organic synthesis [4, 5].

Using first-row transition metals for catalysis that is activated by visible light is very appealing for the development of sustainable synthesis processes because they are typically inexpensive and plentiful [6, 7]. The potential for improved photoluminescent capabilities and the simplicity of synthesis that allows for structural alterations for material property optimization make metal complexes with various ligands interesting materials for optical applications [8-10]. Because of the coordinated metal center or because of changes made to the ligands' backbone substituents, metal complexes produce a wider range of adjustable properties and display their emission color.

*Corresponding authors. E-mail: myelsayed@ju.edu.sa

A rather common event during complexation is the quenching of ligand fluorescence by transition metal ions, which mechanisms like electronic energy transfer, redox activity, magnetic disturbance, etc. can explain. However, it is crucial to enhance fluorescence by complexation in order to open up further photochemical uses for the complexes [11-13].

Excellent spatial and temporal resolution has drawn a lot of interest in fluorescent probes, also referred to as fluorescent chemical sensors [14, 15]. While a number of high-quality fluorescent probes for Cu^{2+}, S^{2-}, and Zn^{2+} sensing have been published [15], research is still ongoing to create new sensors with improved sensitivity, selectivity, and multi-target detection. Because of their large conjugated rigid planar structure and delocalized π-bonds, benzothiazole and its derivatives have excellent optical properties like high fluorescence quantum yield, excellent photostability, and large Stokes shift. For these reasons, they are frequently chosen as fluorescent moieties for a variety of fluorescent probes and sensors [15]. Furthermore, dendritic compounds offer substantial support for efficient sensing due to their diverse intermolecular interactions and repeating three-dimensional structure [15]. Thus, dendron and benzothiazole together make a perfect combination for fluorescent probes.

Besides the biological and medical importance of benzotriazole's [16-19], its usage as a UV stabilizer in polymers and plastics is another important use. Derivatives of BTA absorb ultraviolet light, which stops polymers exposed to sunlight or other UV sources from degrading [20]. Because of this characteristic, BTA is now a crucial ingredient in the manufacturing of outdoor products such plastic films, coatings, and packaging. BTA contributes to extending the performance and lifespan of these materials by preventing UV-induced damage, which lowers waste and enhances sustainability. Additionally, benzotriazole has been used in environmental chemistry, namely for wastewater treatment. Derivatives of BTA have been studied as possible adsorbents for eliminating organic contaminants and heavy metals from water. For example, metal ions including copper, lead, and mercury have been chelated using modified benzotriazole derivatives to reduce their harmful impacts on aquatic ecosystems and stop their release into the environment [21]. The adaptability of benzotriazole and its potential to support environmentally friendly industrial processes are demonstrated by this environmental application. Numerous features are displayed by benzotriazole in several fields. It contributes to improving the mechanical properties of ceramic coatings in material science, where ideal concentrations raise strength and hardness while reducing friction coefficients [22]. The effects of benzotriazole derivatives on geometric parameters, dipole moments, and reactivity have also been the subject of studies; chlorinated derivatives exhibit higher electrophilicity [23]. New fluorescence sensing mechanisms based on photoinduced electron transfer have been made possible using benzotriazole in the manufacture of conjugated polymers, which has resulted in changes in fluorescence emission and enhanced fluorescence quantum efficiency [24]. In addition, benzotriazole [25] and the other fluorescent dyes are used in corrosion inhibitors; its derivatives with hydrophobic shielding layers and improved adsorption capacity are very effective and temperature-resistant, which makes them suitable for a variety of industries applications (e.g. fluorescent markers in biology, analgesics in medicine, sensors, fluorescence switchers, and liquid crystal displays) [26-40].

Because of their strong photostabilizing efficacy, 2-hydroxyphenylbenzotriazole UV absorbers are particularly interesting. They harmlessly disperse the absorbed energy, that is, by converting the absorbed photon energy into heat without undergoing any chemical reactions, and they are transparent to visible light [41]. The main objective of this contribution is to offer a teaching tool for non-specialists in order to pique the reader's interest and encourage more research into this new and exciting area in order to create sustainable future techniques. Considering the aforementioned, we go over the photophysical characteristics of charge transfer metal complexes and how they behave in terms of fluorescence as compared to ligands. Synthesis, thermal behavior analysis, and detection of the coordination power of 2-(2'-hydroxy-5'-phenyl)-5-aminobenzotriazole (hpabt) metal chelates, which contain multiple donor sites are the main

goals of this research. Measurements of molar conductance and magnetic moment support the findings of an investigation into the coordination behavior of hpabt towards transition metal ions. The Fe(III), Cr(III), and V(III) complexes' thermal breakdown were utilized to make structural conjectures; thermal stability analyses are also crucial for their utilization as high-photostability materials.

EXPERIMENTAL

Chemicals and reagents

Every chemical utilized was of the grade of an analytical reagent. These consist of methanol (Fluka), N,N-dimethylformamide (DMF), dimethyl sulphoxide (DMSO) (Fluka), *o*-aminophenol, and *m*-phenylenediamine (Aldrich). Vanadium(III) chloride (VCl_3), ferric chloride hexahydrate ($FeCl_3.6H_2O$), and chromium trichloride hexahydrate ($CrCl_3.6H_2O$) were used exactly as supplied by Aldrich. The supplier of poly(methyl methacrylate) (PMMA) was Aldrich.

Synthesis of hpabt fluorescent dye and its charge transfer metal complexes

With a melting point of 212-215 °C, 2-(2'-hydroxy-5'-phenyl)-5-aminobenzotriazole (hpabt) was created using a previously reported method [42]. By mixing a heated solution of hpabt (0.1 mmol; in 15 mL CH_3OH, 95%) with a corresponding metal(III) chloride salt (0.1 mmol; in 15 mL CH_3OH, 95%), all of the Fe(III), Cr(III), and V(III) of hpabt complexes were created. A hot plate was used to reflux the combinations for 45 min at 60 to 70 °C while stirring them. The Fe(III) complex was brown before the precipitation process, and it turned dark brown when it solidified. Fe(III)-hpabt had a m.p. of >300 °C and an 82% yield. Prior to precipitation, the Cr(III) complex in solution was green; however, it later changed to a dark green precipitate complex with a m.p. >300 °C and a 79% yield. A brownish green precipitate complex with a m.p. >300 °C and a 75% yield was generated in relation to the V(III)-hpabt complex, which had a brown solution color prior to precipitation. In amorphous behavior, every complex is isolated. The dyed polymer matrix was prepared by dissolving PMMA grains and hpabt dye or its metal complexes in chloroform and then mixing them with a magnetic stirrer. After being placed into a glass dish, the uniform mixture was left to dry.

Instrumental analyses

Using a Perkin-Elmer CHN 2400, the contents of carbon, hydrogen, and nitrogen were measured. By directly igniting these complexes at 800 °C for three hours until they reached constant mass, the percentages of iron(III), chromium(III), and vanadium(III) were calculated gravimetrically. After that, the residue was weighed as metal oxides. The Bruker FT-IR Spectrophotometer (4000-400 cm^{-1}) was used to record the infrared spectra of KBr pellets. Using a Jenway 6405 Spectrophotometer with a 1 cm quartz cell, the UV-Vis spectra of the free ligand hpabt and their complexes were conducted in the DMSO solvent at a concentration of 10^{-3} M in the 800–200 nm range.

A Shimadzu 3101pc spectrophotometer was used to perform the solid reflectance spectra. Utilizing the Gouy method, magnetic measurements were performed on a Sherwood Scientific magnetic balance utilizing $[Ni(en)_3](S_2O_3)$ and $Hg[Co(CNS)_4]$ as calibrants. The Jenway 4010 conductivity meter was used to measure the molar conductivities of the freshly made solutions with concentrations of 10^{-3} mol in DMSO. A Shimadzu TGA-50H thermal analyzer was used to perform thermogravimetric studies (TG and DTG) in a dynamic nitrogen environment (30 mL/min) at a heating rate of 10 °C/min. The surface images were obtained utilizing a Scanning Electron Microscopy (SEM) model (specifically the Quanta FEG 250 instrument).

RESULTS AND DISCUSSION

Microanalytical and molar conductance data

The following refers to the chemical reaction pathways involving the interaction of 2-(2'-hydroxy-5'-phenyl)-5-aminobenzotriazole (hpabt) with $MCl_3.nH_2O$ (MCl_3 = VCl_3, $FeCl_3.6H_2O$, and $CrCl_3.6H_2O$) to synthesize hpabt metal complexes. With the general formula $[M(hpabt)(Cl)_3(H_2O)].nH_2O$, the molar ratio for all isolated complexes in solid form is 1:1 (M^{3+} : hpabt). Figure 1 shows the coordination structure of the hpabt complexes. Table 1 contains the elemental analyses, molar conductance, and magnetic measurements data of the hpabt metal chelates, and they are in good agreement with the proposed formulas. Comparing the electrolytic character of each complex with the free hpabt ligand, the molar conductivity values (Λ_m/Ω^{-1} cm^2mol^{-1}) of the free hpabt ligand and their complexes soluble in DMF with 10^{-3} M at 25 °C attested to the non-electrolytic nature of the resulting complexes [43]. Table 1 contains the values of the molar conductance data.

$MCl_3.nH_2O$ + hpabt → $[M(hpabt)(Cl)_3(H_2O)].nH_2O$

Table 1. Data on the molar conductance, magnetic measurements, and elemental analysis of the hpabt complexes.

Complexes Empirical formula, Mwt	Calcd /Found				Molar conductance, $\Omega^{-1}cm^2mol^{-1}$	μ_{eff}, B.M.
	C, %	H, %	N, %	M, %		
hpabt	63.71/ 63.66	4.46/ 4.39	24.76/ 24.65	-	63	-
$[Fe(hpabt)(Cl)_3(H_2O)].4H_2O$, 478.51 g/mol	30.12/ 30.09	4.21/ 4.11	11.71/ 11.64	11.67/ 11.54	72	5.84
$[Cr(hpabt)(Cl)_3(H_2O)].5H_2O$, 492.68 g/mol	29.25/ 29.02	4.50/ 4.36	11.37/ 11.29	10.55/ 10.49	65	3.78
$[V(hpabt)(Cl)_3(H_2O)].H_2O$, 419.57 g/mol	34.35/ 34.27	3.36/ 3.28	13.35/ 13.18	12.14/ 12.05	68	2.85

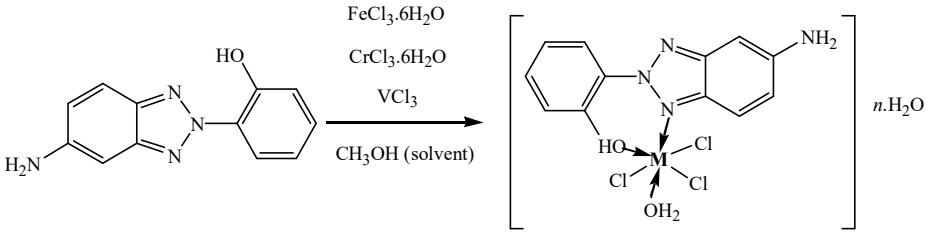

Figure 1. Structure of synthesized hpabt-metal charge transfer complexes. (where, M = Fe^{3+}, Cr^{3+} and V^{3+}).

Electronic absorption spectra and magnetic susceptibility of the hpabt complexes

The hpabt ligand's electronic spectrum shows many bands in the ultraviolet spectrum. The bands in the 230–325 nm region is ascribed to the ligands' π–π* transition. The n–π* electronic transitions are responsible for the remaining bands seen in the 340–575 nm range [44]. The absorption maxima of the three hpabt complexes bears a striking resemblance to the free ligand, suggesting that the ligand's structure was not altered during complexation. However, because the

C=N and OH groups are involved in metal complexation, the values moved slightly to a longer or lower wavelength, and the free ligand did not have two bands at 545 and 575 nm [44].

In solid form, the diffuse reflectance spectrum of the iron(III) complex $[Fe(hpabt)(Cl)_3(H_2O)].4H_2O$ has been obtained. Three absorption bands can be identified in the electronic spectrum iron(III) charge transfer complex at about 19415, 23250, and 25900 cm^{-1}. These bands may be attributed to the transitions $^6A_{1g}\rightarrow{}^4T_{1g}$, $^6A_{1g}\rightarrow{}^4T_{2g}$, $^6A_{1g}\rightarrow{}^4A_{1g}$, and ^4E_g, respectively [44] and indicate octahedral geometry. For the six-coordinated iron(III) system, the magnetic moment of iron(III) complex measured at 5.84 B.M. is in good accord and consistent with the presence of five unpaired electrons [45]. Three spin-allowable transitions at 17500 cm^{-1}, 23950 cm^{-1}, and 37800 cm^{-1} are identified in the absorption spectra of the recently synthesized chromium(III) complex. These transitions can be attributed to the $^4T_{2g}\rightarrow 4A_{2g}$, $^4T_{1g}(F)\rightarrow{}^4A_{2g}$, and $^4T_{1g}(P)\rightarrow{}^4A_{2g}$ transitions, respectively. This supports the chromium(III) complex deformed octahedral shape. The distorted octahedral environment surrounding the metal ion was indicated by the magnetic moment values of the Cr(III) complex, which were found to be in at 3.78 B.M. corresponding to three unpaired electrons [45]. At room temperature, the magnetic moment of the vanadium(III) complex was determined to be 2.85 B.M., which is fairly near to the 2.83 B.M. predicted value for the d^2 system. It indicates the absence of oxidation of the vanadium (III) ion upon complexation [44, 45]. In an octahedral crystal field, the vanadium(III) ion has a d^2 configuration and a ground state of $^3T_{1g}(F)$. The d-d transition $^3T_{1g}(F)\rightarrow{}^3T_{2g}(F)$ is responsible for the band located at 17860 cm^{-1} in the electronic spectra of the $[V(hpabt)(Cl)_3(H_2O)].H_2O$ charge transfer complex. The band at 25975 cm^{-1} in the electronic spectra of V(III) complex can be attributed to the d-d transition of $^3T_{1g}(F)\rightarrow{}^3T_{1g}(P)$ [46].

Infrared spectra

Infrared spectra of the free hpabt ligand (Figure 2) and its Fe(III), Cr(III), and V(III) complexes (Figure 3) were interpreted to provide insight into the chelation mechanism and to monitor the impact of metal ion coordination on the vibration motions of the free ligand.

Table 2. Infrared spectral data assignments of free hpabt ligand and its three Fe(III), Cr(III), and V(III) charge transfer complexes.

hpabt	Complexes			Assignments
	Fe^{3+}	Cr^{3+}	V^{3+}	
3460	-	-	-	ν(O–H)
3377	3141	3228	3271	ν(N–H)
1665	1624	1615	1688	δ_{def}(N–H)
1633 1598	1596	1500	1639 1566	ν(C=N)
1280	-	-	-	δ(O–H) in-plane bending
1250	1262	1281	1247	ν_{as}(C–N)
1161	1156	1145	1102	ν(C–O)
1093	1087	1087	1073	ν_s(C–N)
977	927	893	970	δ_{rock}(N–H)
842	831	835	821	δ_{wag}(N–H)
650	642	675	-	δ(O–H); δ(C–N) out-of-plane bending
-	578	593	656	ν(M–O)
-	506	496	506	ν(M–N)

The free ligand and its metal chelate were subjected to infrared spectra in the mid-IR range of 4000–400 cm^{-1} (Table 2). The aryl-OH group is responsible for a very prominent band at 3460 cm^{-1} in the infrared spectrum of free hpabt ligand [47]. This band is absent in the case of the

Fe(III), Cr(III), and V(III) complexes, which is attributed to the participation of the OH group in the chelating. The NH_2 group stretching vibration band is present in all hpabt complexes as a broad band in conjunction with the uncoordinated water molecules stretching vibration band ν(OH), which makes it challenging to verify the NH_2 group participation in the coordination process. In the free ligand and the complexes, the hypochromic impact (reduction in intensity) of the ν(C–O) stretching band at 1250 cm^{-1} due to substituents or interactions with the molecular environment confirms the shared of the aryl-OH group in coordination [47]. The benzotriazole moiety ν(C=N) caused extremely strong-to-strong bands to appear in the free ligand infrared spectra at 1633 and 1598 cm^{-1} [48]. In complexes that have been impacted by complexation *via* metal ions, this band is pushed to lower/higher frequencies. All hpabt complexes spectra in the 500–400 cm^{-1} area shows bands at around 600 and 440 cm^{-1} [48], which are attributed to the ν(M–O) and ν(M–N) stretching vibrations, respectively. As a result, the IR spectra shows that hpabt functions as a bidentate, with the coordination sites being the benzotriazole ring's ArOH and C=N.

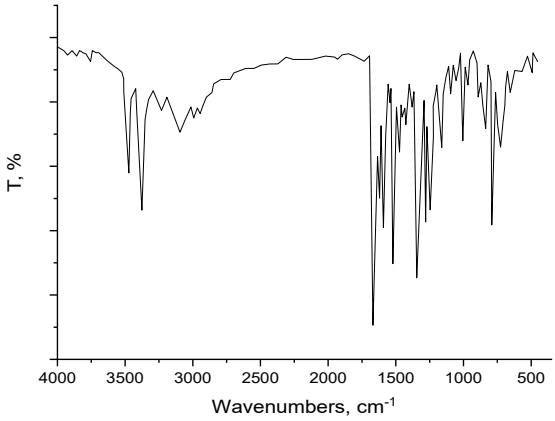

Figure 2. Infrared spectrum of free hpabt ligand.

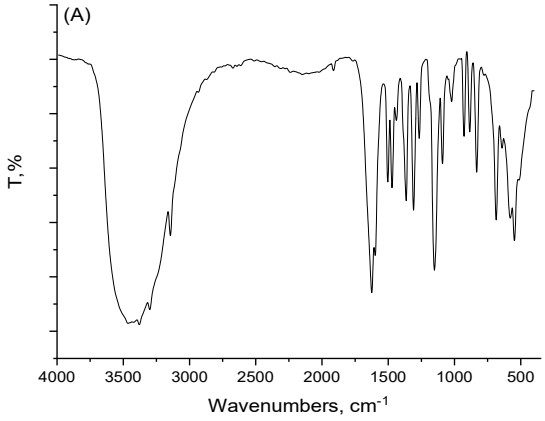

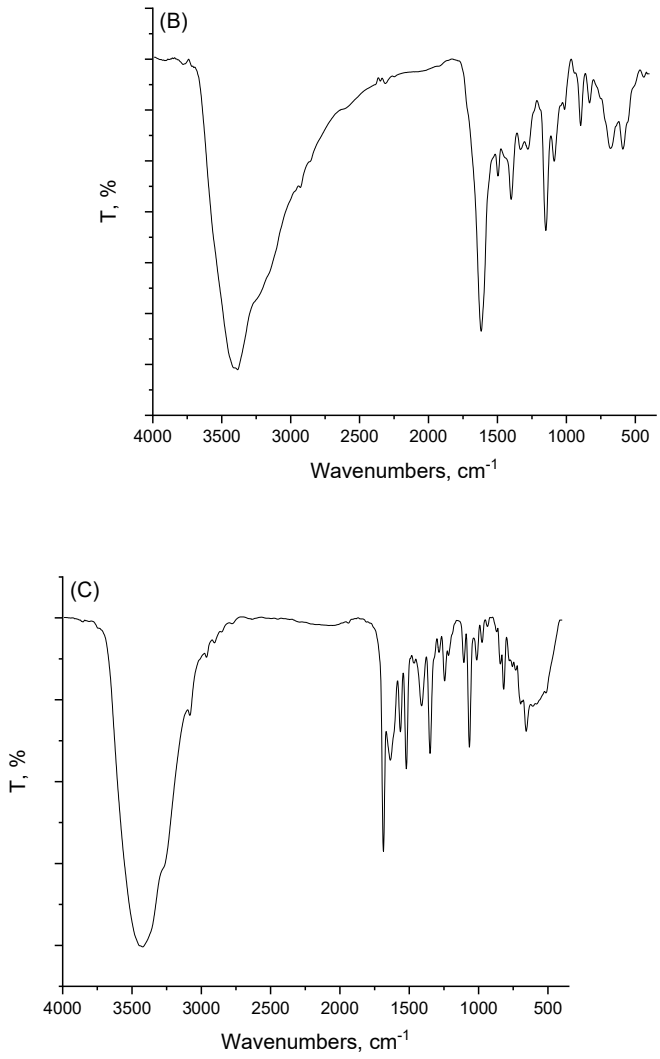

Figure 3. Infrared spectra of (A): $[Fe(hpabt)(Cl)_3(H_2O)].4H_2O$, (B): $[Cr(hpabt)(Cl)_3(H_2O)].5H_2O$, and (C): $[V(hpabt)(Cl)_3(H_2O)].H_2O$ charge transfer complexes.

Thermogravimetric analysis

The following is a study and assignment of the thermal analysis curves of the hpabt and their Fe(III), Cr(III), and V(III) charge transfer metal complexes in Figures 4 and 5. At roughly 212-215 °C, the hpabt ligand melts and simultaneously decomposes. At 261 °C, the first mass loss was noted. The TG curve suggests that the sample breaks down in a single step over the temperature range of 30 to 800 °C. This stage takes place between 150 and 300 °C, and the mass loss from the

loss of $C_{12}H_{10}N_4O$, the difference between the calculated and observed data is (found = 98.50%, calc. = 100.00%).

There are five processes involved in the heat breakdown of the $[Fe(hpabt)(Cl)_3(H_2O)].4H_2O$ complex. The $4H_2O$ molecules in the outside of coordination sphere are removed during the first and second degradation process, which occurs between 30 and 200 ºC and results in a mass loss of (found = 14.80%, calc. = 15.05%). A mass loss of (found = 25.95%, calc. = 26.02%) associated with the third breakdown stage, which occurred between 200 and 400 ºC, was attributed to the loss of three chlorine atoms and the one coordinated H_2O molecule. The fourth and last step of decomposition showed mass loss (found = 42.25%, calc. = 42.24%) and the loss of hpabt organic moiety within the range of 400-700 ºC. The solid residue is $½Fe_2O_3$ (found = 17.00%, calc. = 16.69%), which stable up to 700 ºC. There are three processes involved in the full thermal breakdown of the $[Cr(hpabt)(Cl)_3(H_2O)].5H_2O$ complex. At temperatures between 30 and 250 ºC, $5H_2O$ crystalline molecules were lost, resulting in a mass loss of (found = 18.19%, calc. = 18.27%). The second phase, which takes place between 250 and 400 ºC, relates to the loss of three chlorine atoms and remaining H_2O coordinated water molecules, resulting in a mass loss of (found = 25.16%, calc. = 25.27%). The hpabt moiety decomposes at DTG_{max} = 450 ºC, which takes place between 400 and 700 ºC. The mass loss is (found = 40.96%, calc. = 41.22%). The end products, the $½Cr_2O_3$ and the polluting carbon atoms, are stable up to 700 ºC (found = 15.69%, calc. = 15.43%). There are three primary stages of the $[V(hpabt)(Cl)_3(H_2O)].H_2O$ complex heat degradation. At a maximum temperature of 200 ºC, the first stage of decomposition takes place within 30-250 ºC range. Due to the loss of $2H_2O$ (coordination and uncoordinated) molecules and three chlorine atoms the mass loss associated with this step was found to be (found. = 33.44%, calc. = 33.96%). The temperature peaks for the second and third stages of breakdown are 350 and 550 ºC, respectively. This due to the loss of organic component $C_{12}H_{10}N_4$, which take place at 250–400 ºC and 400–700 ºC (DTG_{max} = 350 and 550 ºC). This results in a mass loss of (found = 47.90%, calc. = 48.18%). At 700 ºC, $½V_2O_3$ (found = 18.66%, calc. = 17.86%) is the last thermal product. Infrared spectra of the last residual products for each hpabt complexes verified that an oxide feature had formed as the result.

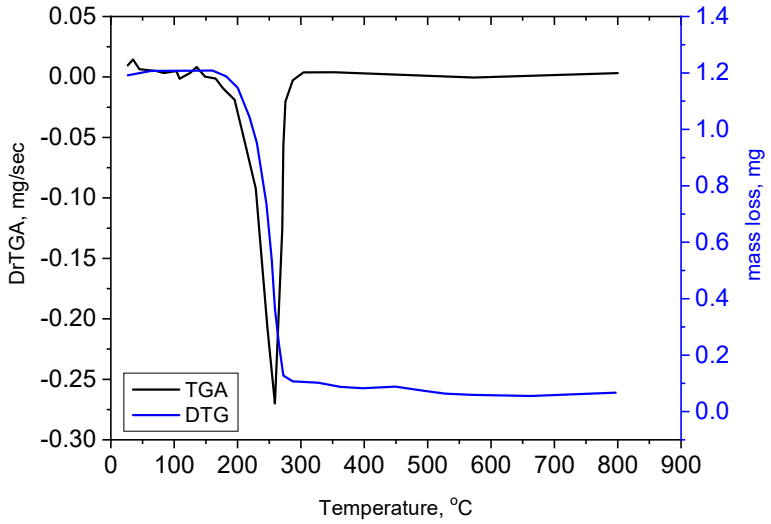

Figure 4. TGA and drTGA curves of free hpabt ligand.

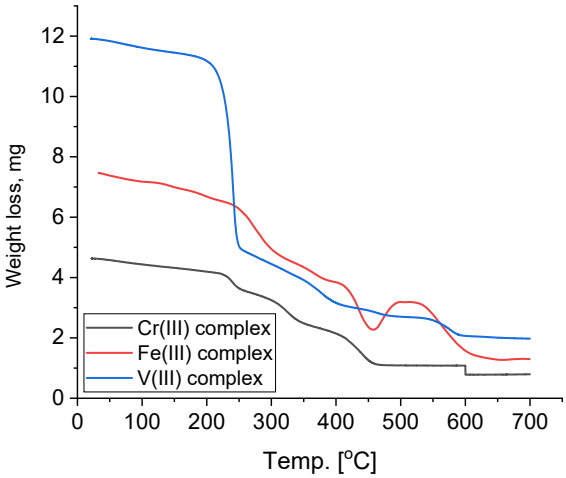

Figure 5. TGA curves of $[Fe(hpabt)(Cl)_3(H_2O)].4H_2O$, $[Cr(hpabt)(Cl)_3(H_2O)].5H_2O$, and $[V(hpabt)(Cl)_3(H_2O)].H_2O$ charge transfer complexes.

Kinetic thermodynamic data

The Coats and Redfern and Horowitz-Metzger equations [49, 50] were used to compute the thermodynamic activation parameters (Table 3) of the initial decomposition step of dehydration, including activation entropy (ΔS*), pre-exponential factor (Z), activation enthalpy (ΔH*), and Gibbs free energy (ΔG*). All complexes had negative entropy (ΔS*) values, indicating that these processes are more ordered. Because of their coordinated bond characteristic, the hpabt complexes high activation energy (E) values demonstrate the high stability of chelation and are also useful in predicting the ligand's binding strength with the metal ions. While ΔS is negative and regarded as unfavorable or non-spontaneous, ΔG is positive. The thermodynamic information derived from the two approaches agrees with one another. A closer approach by the ligand is made possible by the ions reduced size. The Cr(III) complex has a larger "E" value than the other Fe(III) and V(III) complexes as a result, because of the ionic radius of the Cr(III) complex decreases, so it is anticipated that energy activation will rise. The thermal decomposition steps' Arrhenius plots showed a satisfactory fit with a linear function, with correlation coefficients falling between 0.9965 and 0.9932.

Table 3. Kinetic and thermodynamic parameters of the thermal decomposition of hpabt metal complexes.

Complex	r	Z s^{-1}	T_{max} (K)	E_a kJ.mol^{-1}	ΔS^* J.K^{-1}mol^{-1}	ΔH^* kJ.mol^{-1}	ΔG^* kJ.mol^{-1}
Fe(III)	0.9965	$2.82*10^5$	460	36.42	-140.60	32.22	86.73
Cr(III)	0.9950	$2.10*10^6$	450	48.50	-126.66	44.48	90.82
V(III)	0.9932	$1.65*10^5$	350	38.29	-145.90	34.35	87.24

Scanning electron microscopy investigation

The SEM images of the synthesized Fe(III), Cr(III), and V(III) complexes are shown in Figure 6. The consistency and resemblance of the synthetic complexes actual sizes, shapes, and forms, show

that all complexes with morphological phases have an inhomogeneous matrix. Small to medium-sized particles of various shapes are present in the inhomogeneous phase development of the synthesized Fe(III), Cr(III), and V(III) complexes. Smaller particles attach to the longer particles, which show a wide particle size distribution with irregularly shaped particles with smooth surfaces. Small to medium-sized particles with the shape of rock blocks make up the Fe(III) complex, Figure (6A), and the resulting practical had a smooth surface. The small-to-medium variant particles have an average diameter of 5 μm. Small to big particles with unusual long and wide line forms make up the Cr(III) complex, Figure (6B), and the resulting practical had a smooth surface. It is discovered that the small-to-larger variation particles have an average diameter of about 10 μm. Small-to-larger particles with an uneven coral reef form are present in the V(III) complex, Figure (6C), and the resulting practical had a rough surface. The change of free hpabt geometric nanoparticles into bigger inhomogeneous nanoparticles upon the combination with Fe(III), Cr(III), and V(III) ions is the result's importance, it can be concluded.

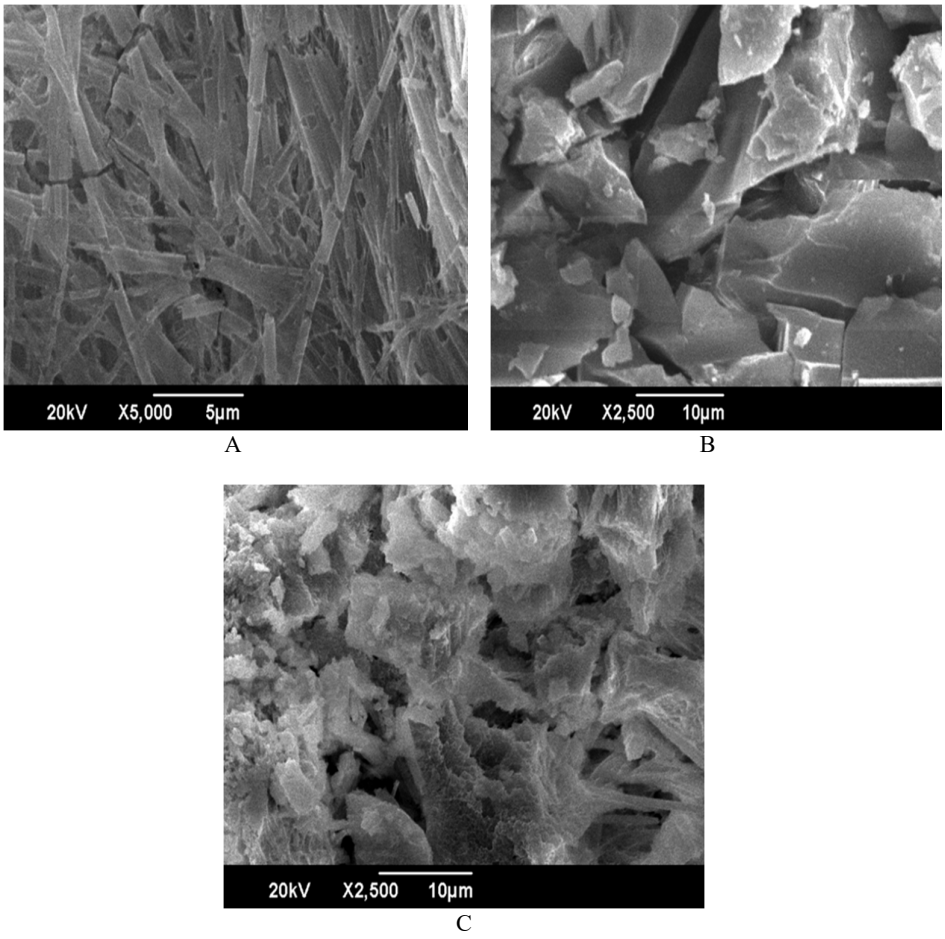

A B C

Figure 6. SEM images of (A): $[Cr(hpabt)(Cl)_3(H_2O)].5H_2O$, (B): $[Fe(hpabt)(Cl)_3(H_2O)].4H_2O$ and (C): $[V(hpabt)(Cl)_3(H_2O)].H_2O$ charge transfer complexes.

Photostability study

After extended exposure to sunshine, all organic dyes fade, as is widely known. In this regard, the dyes used in fluorescent collectors must meet rigorous requirements. Solar collectors are supposed to last 10 to 20 years, yet many dyes fade in broad sunshine in a matter of hours or days. Fluorescent collectors should aim for a dye lifetime of five years since the solar cells, which are the costliest component of the system, may remain in place and not deteriorate while the collector plates are changed periodically. A few factors affect the photostability of dyes: (i) Manufacturing factors like plastic material additives, polymerization process, post-polymerization treatment, and dye concentration. (ii) Operational factors like temperature under illumination, temperature during periods without illumination, incident light spectrum, and incident light intensity.

The 2-(2'-hydroxy-5'-phenyl)-5-aminobenzotriazole (hpabt) fluorescent dye doped in PMMA can only degrade photochemically when appropriate optical light (UV lamp power) is present. This causes significant local temperature increases and thermals fade away from the dye molecules. Table 4 shows the change in the absorption spectra at various points during the irradiation period for hpabt and ($[Cr(hpabt)(Cl)_3(H_2O)].5H_2O$, $[Fe(hpabt)(Cl)_3(H_2O)].4H_2O$ and $[V(hpabt)(Cl)_3(H_2O)]\ .H_2O$ charge transfer complexes) doped in PMMA that were exposed inside to UV-Vis. radiation. Following complexation, photostability is enhanced by Metal-to-Ligand charge transfer complexation. The following formula [25, 31, 32, 34, 42] was used to estimate the rate constant of dye photodegradation.

$$k = \frac{2.303}{t} \log \frac{A_0}{A} \qquad (1)$$

$$t_{½} = \frac{0.693}{k}$$

where the absorptions for time (t) before and after irradiation are denoted by A_0 and A. Table 4 lists the half-life times and the k value. The degradation data makes it evident that the complexations alter the dye's photostability.

Table 4. Half-life times ($t_{½}$) and rate constants/k of photodegradation of $[Cr(hpabt)(Cl)_3(H_2O)].5H_2O$, $[Fe(hpabt)(Cl)_3(H_2O)].4H_2O$ and $[V(hpabt)(Cl)_3(H_2O)]\ .H_2O$ charge transfer complexes doped in PMMA.

Samples	Parameters		
	Wavelength, λ_{nm}	k/ min^{-1}	$t_{½}$/ min
$[Cr(hpabt)(Cl)_3(H_2O)].5H_2O$	412 nm	4.14×10^{-5}	16756
$[Fe(hpabt)(Cl)_3(H_2O)].4H_2O$	445 nm	5.34×10^{-5}	12980
$[V(hpabt)(Cl)_3(H_2O)].H_2O$	423 nm	6.50×10^{-5}	10661

It is evident under a UV lamp that the $[Cr(hpabt)(Cl)_3(H_2O)].5H_2O$ complex exhibits greater photostability than the other $[Fe(hpabt)(Cl)_3(H_2O)].4H_2O$ and $[V(hpabt)(Cl)_3(H_2O)].H_2O$ charge transfer complexes. The photostability properties of 2-(2'-hydroxy-5'-phenyl)-5-aminobenzotriazole (hpabt) are found to be enhanced by chromium(III) ions instead of iron(III) and vanadium(III) ions.

CONCLUSION

Metal complexes formed from the reaction of 2-(2'-hydroxy-5'-phenyl)-5-aminobenzotriazole with some transition metal salts as acceptors have been studied. The final reaction products have been isolated and characterized using electronic (UV – Vis), mid infrared spectra and thermal

measurements as well as elemental analysis CHN. The chemical analysis data of the resulted metal complexes reveal that the formation of a 1:1 metal complex in case of iron(III), chromium(III), and vanadium(III) metal ions. The kinetic thermodynamic parameters are calculated from the TGA diagrams using both coats-Redfern and Horowitz-Metzger methods. In our work we added modification to enhance the photostability and good efficiency of fluorescent solar collectors, by increasing the photostability of the 2-(2'-hydroxy-5'-phenyl)-5-aminobenzotriazole dye by operated metal complexes reactions.

ACKNOWLEDGEMENT

This work was funded by the Deanship of Graduate Studies and Scientific Research at Jouf University under grant No. (DGSSR-2024-02-01089).

REFERENCES

1. Roth, H.D. The beginnings of organic photochemistry. *Angew. Chem. Int. Ed. Engl.* **1989**, 28, 1193-1207.
2. Marzo, L.; Pagire, S.K.; Reiser, O.; König B. Visible-light photocatalysis: Does it make a difference in organic synthesis? *Angew. Chem. Int. Ed. Engl.* **2018**, 57, 10034-10072.
3. McAtee, R.C.; Edward, J.M.; Stephenson, C.R. Illuminating photoredox catalysis. *Trends Chem*. **2019**, 1, 111-125.
4. Candish, L.; Collins, K.D.; Cook, G.C.; Douglas, J.J.; Gómez-Suárez, A.; Jolit, A.; Keess, S. Photocatalysis in the life science industry. *Chem. Rev*. **2021**, 122, 2907-2980.
5. Spencer, P.P.; Larry, E.O. Strategic use of visible- light photoredox catalysis in natural product synthesis. *Chem. Rev*. **2022**, 122, 1717-1751.
6. Hayler, J.D.; Leahy, D.K.; Simmons, E.M. A pharmaceutical industry perspective on sustainable metal catalysis. *Organometallics* **2018**, 38, 36-46.
7. Bullock, R.M.; Chen, J.G.; Gagliardi, L.; Chirik, P.J.; Farha, O.K.; Hendon, C.H.; Jones, C.W.; Keith, J.A.; Klosin, J.; Minteer, S.W.; Morris, R.H.; Radosevich, A.T.; Rauchfuss, T.B.; Strotman, N.A.; Vojvodic, A.; Ward, R.R.; Yang, J.Y.; Surendranath, using natures blueprint to expand catalysis with earth-abundant metals. *Sci.* **2020**, 369, eabc3183.
8. Bu, J.; Duan, H.; Wang, X.J. Fluorescence sensors for Cu^{2+} based on con jugated indole Schiff base. *Res. Chem. Intermed.* **2014**, 138, 3119-3126.
9. Paul, B.K.; Kar, S.; Guchhait, N. A Schiff base-derived new model compound for selective fluorescence sensing of Cu(II) and Zn(II) with ratiometric sensing potential: Synthesis, photophysics and mechanism of sensory action. *J. Photochem. Photobiol. A: Chem.* **2011**, 220, 153-163.
10. Li, Y.; Wang, B.; Yang, Z. Infrared and DNA-binding on ultraviolet and fluorescence spectra of new copper and zinc complexes with a naringenin Schiff-base ligand. *Spectrochim. Acta A Mol. Biomol. Spectrosc*. **2007**, 67, 395-401.
11. David, S.S.; Meggers.E. Inorganic chemical biology: from small metal complexes in biological systems to metalloproteins. *Curr. Opin. Chem. Biol.* **2008**, 12, 194-196.
12. Aksuner, N.; Henden, E.; Yilmaz, I.A highly sensitive and selective fluorescent sensor for the determination of copper(II) based on a Schiff base. *Dyes Pigm.* **2009**, 83, 211-217.
13. Li, L.; YQ Dang, Y.Q.; Li, H.W. Fluorescent chemosensor based on Schiff base for selective detection of zinc (II) in aqueous solution. *Tetrahedron Lett*. **2010**, 51, 618-621.
14. Linxiu, Z.; Junli, S.; Yongzheng, L.; Mingfeng, H.; Shengling, L.; Duanlin, C. Novel benzothiazole-based fluorescent probe for efficient detection of Cu^{2+}/S^{2-} and Zn^{2+} and its applicability in cell imaging. *Anal. Chim. Acta* **2024**, 1324, 343093-343098
15. Toshiyuki, U.; Tomoyuki, I.; Ryuhei, S.; Takeshi, M.; Shigeyuki, Y. Fluorescent 2-phenyl-2H-benzotriazole dyes with intramolecular N–H···N hydrogen bonding: Synthesis and

modulation of fluorescence properties by proton-donating substituents. *Dyes Pigm.* **2020**, 183, 108672-108679.
16. Alakeel, A.O. Synthesis and antimicrobial activity of novel benzotriazole derivatives. *Antibiotics* **2021**, 10, 1098-1109.
17. Martins, F.N. Antifungal properties of halogenated benzotriazole derivatives. *Fungal Biol.* **2022**, 126, 87-96.
18. Pasparakis, M. NF-KB regulation in inflammation and disease. *Cell*. **2020**, 181, 23-43.
19. Zhengrong, Y.; Chuan, G.; Chang, L.; Xinggang, L.; Ward, R.M. Advanced corrosion protection using benzotriazole derivatives. *Corro. Sci.* **2020**, 171, 108715-108732.
20. Yu, M. UV stabilizers in polymers: A review of benzotriazole derivatives. *J. Appl. Polym. Sci.* **2021**,138, 51125-51135.
21. Yang, M. Environmental applications of benzotriazole-based adsorbents for heavy metal removal. *Chemosphere* **2021**, 280, 130743-130750.
22. Xin, X. Ultrafast and selective labeling of endogenous proteins using affinity-based benzotriazole chemistry. *Chem. Sci.* **2022**, 13, 7240-7246.
23. Shanaghi, A.; Souri, A.R.; Rafie, M.; Chu, P.K. Effects of Benzotriazole on nano-mechanical properties of zirconia–alumina–Benzotriazole nanocomposite coating deposited on Al 2024 by the sol–gel method. *Appl. Phys. A* **2019**, 125, 728-739.
24. Manzur, M.E.; Iramain, M.A.; Darugar, V.; Vakili, M.; Brandán, S.A. Impact of different groups on properties of all members of the series of 1-X-benzotriazole derivatives (X = H, OH, NH_2, Cl and CH_3). *Eur. J. Theor. Appl. Sci.* **2023**, 1, 406-440.
25. Luo, H. Energy band gap modulation and photoinduced electron transfer fluorescence sensing properties of D–A conjugated polymers containing benzotriazole. *J. Polym. Sci.* **2024**, 62, 200-218.
26. Martin, E.; Weigand, R.; Pardo, A. Solvent dependence of the inhibition of intramolecular charge-transfer in N-substituted 1,8-naphthalimide derivatives as dye lasers. *J. Lumin.* **1996**, 68, 157-64.
27. Tao, Z.F.; Qian, X. Naphthalimide hydroperoxides as photonucleases: substituent effects and structural basis. *Dyes Pigm.* **1999**, 43, 139-145.
28. Zheng, Y.M.; An, Z.X.; Zhao, X.E.; Quan, F.S.; Zhao, H.Y.; Zhang, Y.R.; Liu, J.; He, X.Y.; He, X.N. Comparation of enhanced green fluorescent protein gene transfected and wild-type porcine neural stem cells. *Res. Veterinary Sci*. **2010,** 88, 88-93.
29. de Souza, M.M.; Correa, R.; Cechinel, F.V.; Grabchev, I.; Bojinov, V. 4-Nitro-1,8-naphthalimides exhibit antinociceptive properties. *Pharmazie* **2002**, 56, 430-439.
30. Facoetti, H.; Robin, P.; Le Barny, P.; Schott, M.; Bouche, C.M.; Berdague, P. Side-chain electroluminescent polymers. *Synth Met.* **1996**, 81, 191-196.
31. Grabchev, I.; Chovelon, J.M.; Qian, X. A copolymer of N,Ndimethylaminoethylene-*N*-allyl-1,8-naphthalimide with methylmethacrylate as a selective fluorescent chemosensor in homogeneous systems for metal cations. *J. Photochem. Photobiol. A: Chem.* **2003**, 158, 37-43.
32. Poteau, X.; Brown, A.; Brown, R.; Holmes, C.; Matthew, D. Fluorescence switching in 4-amino-1,8-naphthalimides: "on–off–on" operation controlled by solvent and cations. *Dyes Pigm.* **2000**, 47, 91-105.
33. Zhu, W.; Hu, M.; Yao, R.; Tian, H. A novel family of twisted molecular luminescent materials containing carbazole unit for single-layer organic electroluminescent devices. *J. Photochem. Photobiol. A: Chem.* **2003**, 154, 169-177.
34. Grabchev, I.; Moneva, I.; Wolarz, E.; Bauman, D. New unsaturated 1,8-naphthal-imide dyes for use in nematic liquid crystals. *Z Naturforsch*. **1996**, 51a, 1185-1191.
35. Cosnard, F.; Wintgens, V. A new fluoroionophore derived from 4-amino-N-methyl-1,8-naphthalimide. *Tetrahedron Lett.* **1998**, 39, 2751-2755

36. Zollinger, H. *Color Chemistry Syntheses, Properties, and Applications of Organic Dyes*.: VCH: Weinheim; **1987**.
37. Nishihara, H. Multi-mode molecular switching properties and functions of azo-conjugated metal complexes. *Bull. Chem. Soc. Jpn.* **2004**, 77, 407-435.
38. Geng, Y.; Gu, D.; Gan, F. Application of novel azo metal thin film in optical recording. *Opt. Mater.* **2004**, 27, 193-200.
39. Bin, W.; Yi-Qun, W.; Dong-Hong, G.; Fu-Xi, G. Optical parameters and absorption of azo dye and Its metal-substituted compound thin films. *Chin. Phy. Lett.* **2003**, 20, 1596-1599.
40. Ranby, B.; Rabek, J. *Photodegradation, Photooxidation and Photostabilization of Polymers*, Wiley: London; **1975**.
41. Crawford, J.C. 2(2-hydroxyphenyl)2H-benzotriazole ultraviolet stabilizers. *Prog. Polym. Sci*. **1999**, 24, 7-43.
42. Bojinov, V.; Grabchev, I. Synthesis and properties of new adducts of 2,2,6,6-tetramethylpiperidine and 2-hydroxyphenylbezotriazole as polymer photostabilizers. *J. Photochem. Photobiol. A: Chem*. **2002**, 150, 223-254.
43. Refat M.S. Complexes of uranyl(II), vanadyl(II) and zirconyl(II) with orotic acid "vitamin B13": Synthesis, spectroscopic, thermal studies and antibacterial activity. *J Mol Str.* **2007**, 842, 24-37.
44. Lever A.B.P. *Inorganic Electronic Spectroscopy*, 1st ed., Elsevier: Amsterdam; **1968**.
45. Cotton, F.A.; Wilkinson, G. *The Element of First Transition Series Advanced Inorganic Chemistry*. 3rd ed., John Wiley and Sons: New York; **1992**.
46. Condren, S.M.; McDonald, H.O. The synthesis and spectroscopic properties of vanadium(III) squarate trihydrate. *Inorg. Chem*. **1973**, 12, 57-59.
47. Nakanishi, K.; Solomon, P.H. *Infrared Absorption Spectroscopy*, 2nd ed., Holden-Day, Inc.: USA; **1977**.
48. Karipcin, F.; Kabalcilar, E. Spectroscopic and thermal studies on solid complexes of 4-(2-pyridylazo) resorcinol with some transition metals. *Acta Chim. Slov*. **2007**, 54, 242-247.
49. Coats, A.W.; Redfern, J.P. Kinetic parameters from thermogravimetric data. *Nat.* **1964**, 201, 68-69.
50. Horowitz, H.W.; Metzger, G. A new analysis of thermogravimetric traces. *Anal. Chem*. **1963**, 35, 1464-1472.